

The Optimal Control of Unsteady Flows with a Discrete Adjoint Method

Markus P. Rumpfkeil

University of Toronto Institute for Aerospace Studies, Toronto, Ontario, Canada
email: markus@oddjob.utias.utoronto.ca

David W. Zingg

University of Toronto Institute for Aerospace Studies, Toronto, Ontario, Canada
email: dwz@oddjob.utias.utoronto.ca

Abstract. This paper presents a general framework to derive a discrete adjoint method for the optimal control of unsteady flows. The complete formulation of a generic time-dependent optimal design problem is introduced and it is outlined how to derive the discrete set of adjoint equations in a general approach. Results are shown that demonstrate the application of the theory to the drag minimization of viscous flow around a rotating cylinder, and to the remote inverse design of laminar flow around the multi-element NLR 7301 configuration at a high angle of attack. In order to reduce the considerable computational costs of unsteady optimization, the use of bigger time steps over transitional or unphysical adjusting periods as well as the skip of time steps while recording the flow solution are investigated and are shown to work well in practice.

Keywords: computational fluid dynamics, optimization, unsteady flow, discrete adjoint method, optimal control, remote inverse design, rotating cylinder

1. Introduction and Motivation

The use of steady-state aerodynamic optimization methods in the computational fluid dynamics (CFD) community is fairly well established (Obayashi, 1997; Jameson et al., 1998; Anderson and Bonhaus, 1999; Nemec and Zingg, 2002). In particular the use of adjoint methods, which has been pioneered by Jameson (1995) for steady aeronautical design optimization, has proved to be very beneficial since its cost is independent of the number of design variables. However, a much smaller amount of work has been done in applying these methods to unsteady optimization problems (Nadarajah and Jameson, 2002; Duta et al., 2002; Tatossian and Nadarajah, 2007; Mani and Mavriplis, 2007), and many devices of interest, such as helicopter rotors and turbomachinery blades, operate in unsteady flow environments.

Similarly, the application of numerical optimization to airframe-generated noise has not received much attention either, but with the significant quieting of modern engines, airframe noise now competes with engine noise (Singer et al., 2000). Thus airframe-generated noise



is an important component of the total noise radiated from commercial aircraft, especially during aircraft approach and landing, when engines operate at reduced thrust, and airframe components (such as high-lift devices) are in the deployed state (Khorrami et al., 2000). Future Federal Aviation Administration noise regulations, the projected growth in air travel, and the increase in population density near airports will require future civil aircraft to be substantially quieter than the current ones. Consequently, the attempt to understand and reduce airframe noise has become an important research topic (Singer and Guo, 2004).

In this paper, a framework to calculate the gradient of an objective function in a nonlinear unsteady flow environment via the discrete adjoint method is developed in Section 2. It is then applied to two model problems to show its effectiveness, namely to the drag minimization of viscous flow around a rotating cylinder in Section 3.1 and to the remote inverse design of unsteady laminar flow around the National Aerospace Laboratory NLR 7301 configuration (van den Berg, 1979) at a high angle of attack in Section 3.2. This framework can also be used to optimize the shapes of helicopter rotors or turbomachinery blades and for many other inherently unsteady optimization problems. The eventual goal of this research is to be able to modify the shape of a multi-element airfoil to minimize the radiated noise during approach while maintaining good performance. The presented remote inverse design problem in Section 3.2 is a major milestone toward this goal.

However, the optimal control of time-dependent problems is in general a computationally expensive task since one needs to solve the adjoint equations in reverse time from a final flow solution. Thus one has to store the entire flow history, which means potentially huge memory requirements, and then to integrate the adjoint equations backwards in time which leads to equally huge processor requirements (Nadarajah and Jameson, 2002). This issue is addressed in this paper by the use of an increased time step over transitional or unphysical adjusting periods as well as omitting time steps while recording the flow solution.

2. Formulation of the Discrete Time-dependent Optimal Control Problem

The control of an unsteady flow in the time interval $[0, T]$ is considered. The initial flow solution Q^0 at $t = 0$ must be known and for the discrete adjoint method the time discretization scheme for the governing equations must be chosen at this point in the derivation. The framework is demonstrated here using the implicit Euler time-marching method. It is straightforward to modify the equations to use any other time-

marching method (e.g. see the Appendix for the derivation with the second-order backwards difference (BDF2) time-marching method as used in Section 3).

Now one introduces a cost function

$$J = \sum_{n=1}^N I^n(Q^n, Y), \quad (1)$$

where the function $I^n = I^n(Q^n, Y)$ depends on the time-dependent flow solution Q^n and design variables Y for $n = 1, \dots, N$. N can be calculated from the relation $T = N\Delta t$, where Δt is the chosen time discretization step. The time-dependent flow solution Q^n for $n = 1, \dots, N$ can be implicitly defined via

$$R^{*n}(Q^n, Q^{n-1}, Y) := \frac{dQ^n}{dt} + R(Q^n, Y) = \frac{Q^n - Q^{n-1}}{\Delta t} + R(Q^n, Y) = 0, \quad (2)$$

where $R = R(Q^n, Y)$ contains the spatially discretized convective and viscous fluxes as well as the boundary conditions. We use an inexact Newton strategy to drive $R^{*n} = R^{*n}(Q^n, Q^{n-1}, Y)$ to zero (Isono and Zingg, 2004; Pueyo and Zingg, 1998). However, it does not matter how one solves equation (2) as long as $R^{*n} = 0$ for all n , since this is the requirement for the following derivation.

The task of minimizing the cost function J subject to $R^{*n} = 0$ for all n can now be written as an unconstrained optimization problem of minimizing the Lagrangian function

$$\mathcal{L} = \sum_{n=1}^N [I^n(Q^n, Y) + (\psi^n)^T R^{*n}(Q^n, Q^{n-1}, Y)] \quad (3)$$

with respect to Q^0, \dots, Q^N and ψ^1, \dots, ψ^N , where ψ^1, \dots, ψ^N are the N vectors of Lagrange multipliers. A necessary condition for an extremal is that the gradient of \mathcal{L} with respect to Q^0, \dots, Q^N and ψ^1, \dots, ψ^N should vanish. Since the states Q^1, \dots, Q^N are calculated starting from Q^0 using the constraints given by equation (2), it is automatically guaranteed that $\nabla_{\psi^n} \mathcal{L} = 0$ for $n = 1, \dots, N$.

The Lagrange multipliers ψ^n must now be chosen such that $\nabla_{Q^n} \mathcal{L} = 0$ for $n = 1, \dots, N$, which leads to

$$0 = \nabla_{Q^n} I^n + (\psi^n)^T \nabla_{Q^n} R^{*n} + (\psi^{n+1})^T \nabla_{Q^n} R^{*n+1} \quad (4)$$

for $n = 1, \dots, N-1$

$$0 = \nabla_{Q^N} I^N + (\psi^N)^T \nabla_{Q^N} R^{*N}. \quad (5)$$

This can be written equivalently as

$$\psi^N = - ((\nabla_{Q^N} R^{*N})^T)^{-1} (\nabla_{Q^N} I^N)^T \quad (6)$$

$$\begin{aligned} \psi^n = & - \left((\nabla_{Q^n} R^{*n})^T \right)^{-1} \left[(\nabla_{Q^n} I^n)^T + (\nabla_{Q^n} R^{*n+1})^T \psi^{n+1} \right] \\ \text{for } n = & N-1, \dots, 1. \end{aligned} \quad (7)$$

Since Q^1, \dots, Q^N have been calculated from the current guess of Y , the vectors of Lagrange multipliers ψ^n can be calculated recursively backwards from the final flow solution (6) using (7). The system of equations (6) and (7) is known as the system of adjoint equations for the model (2), or as the adjoint model. In this context, the Lagrange multipliers are also known as the adjoint variables.

Finally, one can evaluate the gradient of J with respect to the design variables Y , which can then be used in a gradient-based optimization algorithm such as BFGS (Broyden, 1970; Fletcher, 1970; Goldfarb, 1970; Shanno, 1970) to find the optimum:

$$\frac{\partial J}{\partial Y} = \frac{\partial \mathcal{L}}{\partial Y} = \sum_{n=1}^N \left[\nabla_Y I^n(Q^n, Y) + (\psi^n)^T \nabla_Y R(Q^n, Y) \right]. \quad (8)$$

In summary, the gradient is determined by the solution of the adjoint equations in reverse time from the final flow solution and the partial derivatives of the discretized fluxes and objective function with respect to the design variables (while Q^n is held constant). One can also see that the computational costs of unsteady optimization problems are directly proportional to the desired number of time steps and (almost) independent of the number of design variables.

3. Results

We now present the two examples to demonstrate how this framework can be applied in practice. We use the preconditioned Bi-CGSTAB algorithm (van der Vorst, 1992) with an absolute convergence tolerance of 10^{-12} in order to solve the linear systems in the adjoint equations. We find that Bi-CGSTAB is about fifty percent faster than the preconditioned generalized minimum residual (GMRES) method (Saad and Schultz, 1986), which we use in our flow solvers in conjunction with an inexact Newton strategy (Pueyo and Zingg, 1998). The reason for this is most likely the fact that $(\nabla_{Q^n} R^{*n})^T$ is more diagonally dominant than the steady flow Jacobian $(\nabla_Q R)^T$ due to the extra terms on the diagonal, which makes this matrix more suited for the use of Bi-CGSTAB. However, for the unsteady flow solvers we still use the GMRES method because there are no significant computational savings for the few linear iterations we use per nonlinear (outer) iteration.

3.1. DRAG MINIMIZATION FOR VISCOUS FLOW AROUND A ROTATING CYLINDER

The viscous flow past a circular cylinder has been comprehensively studied due to its simple geometry and its representative behavior of general bluff body wakes. There are various flow regimes which are highly dependent on the Reynolds number (Re) and can be identified by the character of the flow in the wake and boundary layer of the cylinder (Cox et al., 1998). However, over a large Reynolds number range ($47 < Re < 10^7$) there are always eddies shed alternately from each side of the cylinder, forming rows of vortices in its wake, the so-called Karman vortex street (von Karman, 1911).

Using the Magnus Effect (also known as the Robin's Effect), which can be observed for rotating spheres as well as cylinders, one can try to suppress the Karman vortex shedding by controlling the angular velocity of the rotating body. A deep understanding of the control strategies for flows past rotating bluff bodies is very helpful in areas such as drag reduction, lift enhancement, vibration control and last but not least, our particular interest, noise control.

In order to solve the underlying 2D unsteady Navier-Stokes equations, we use our 2D single-block structured thin-layer solver, PROBE (Pueyo and Zingg, 1998), which is a Newton-GMRES solver loosely based on ARC2D (Pulliam, 1986). The rotational boundary conditions are implemented by requiring the normal velocity on the surface of the cylinder to be zero and the tangential velocity to be equal to $\Omega \cdot r$, where Ω is the angular velocity and $r = 0.5$ the radius of the cylinder.

It is convenient to introduce the Strouhal number

$$S_n = d \cdot f_n / u_\infty$$

for comparison purposes, where d is the diameter of the cylinder, f_n is the Karman vortex shedding frequency, and u_∞ is the free-stream velocity. Using an O-mesh with 140×90 grid nodes and the BDF2 time-marching method with a time step of $\Delta t = 0.1$, we compare our results for the mean value of the drag coefficient \bar{C}_D and the Strouhal number S_n with experimentally and computationally obtained values by various authors (Homescu et al., 2002; He et al., 2000; Williamson, 1989; Henderson, 1997) in Table I.

There is a reasonable agreement for both Reynolds numbers. We recognize that our time steps are relatively large and the grid is relatively coarse. Also, the use of the thin-layer Navier-Stokes equations is questionable for a bluff-body flow and will deviate to some degree from a full Navier-Stokes solution. However, since the primary focus of this paper is on the optimal control of unsteady flows, we are satisfied with

Table I. Mean drag coefficients and Strouhal numbers.

Reynolds number	\bar{C}_D		S_n	
	100	1000	100	1000
Present work	1.45	1.53	0.179	0.252
Homescu et al. (2002)	1.42	1.68	-	-
He et al. (2000)	1.35	1.52	0.167	0.239
Williamson (1989)	-	-	0.164	-
Henderson (1997)	1.35	1.51	0.166	0.237

the trade-off between accuracy and performance and we proceed, even though the computed unsteady flow is not grid converged in this case.

The experimental work of Tokumaru and Dimotakis (1991) motivates the attempt to find an optimal angular velocity in order to minimize the drag. Several researchers (Homescu et al., 2002; He et al., 2000) have considered two control cases (but used different objective functions): The constant rotation case, $\Omega(t) = \Omega$ using $Y = \Omega$ as design variable, and the time harmonic rotary oscillation case, $\Omega(t) = A \cdot \sin(2\pi Ft)$ with $Y = (A, F)$ as design variables.

Our choice for the objective function for the constant and harmonic rotating cases is a time average (mean) drag minimization problem:

$$J = \bar{C}_D = \frac{1}{N - N^*} \sum_{n=N^*+1}^N C_D^n, \quad (9)$$

where C_D^n is the drag coefficient at time step n .

It is very important to have a practical knowledge of the design space to be able to choose a reasonable time step and control window. Therefore, the effect of different values of Ω on the drag coefficient for the constant rotation case using a fixed time step of $\Delta t = 0.1$ is shown in Figure 1. The rotation starts impulsively, and after a transition period of about 1500 steps the mean drag coefficients of the rotating cylinders are all smaller than the mean drag coefficient of the stationary cylinder.

In order to reduce the computational costs in the actual optimization runs we “jump” over the adjusting or transition period as quickly as possible by taking a bigger time step $\Delta T = 0.5$ for $N^* = 300$ steps. This larger time step is chosen in such a way that the accuracy of the overall numerical solution is not significantly diminished. Once we reach the domain where we want to control the problem (the control window is indicated by the box in Figure 1), we use a smaller time step $\Delta t = 0.2$ for another 500 steps, for a total of $N = 800$ time steps in each flow solve. The corresponding adjoint equations for this situation are given in the Appendix.

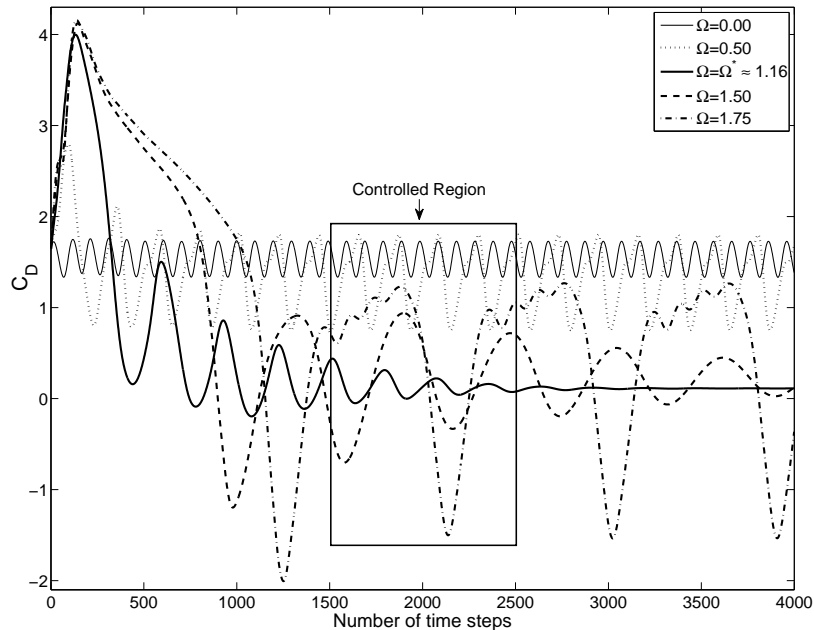


Figure 1. Drag coefficients for the constant rotation case for different values of Ω ($\Delta t = 0.1$).

Using BFGS (Zhu et al., 1994; Byrd et al., 1995) and constraining Ω to values between 0 and 1.9, we are able to minimize the mean drag with gradient norms of 10^{-8} at the local minima. The resulting design space is shown in Figure 2 with the gradients at the design points represented as straight lines. One can see several local minima in this design space, with the global minimum in the given interval at $\Omega = \Omega^* \approx 1.16$ leading to $\bar{C}_D \approx 0.11$. This optimum value minimizes the mean drag value far beyond the extent of the control window, as can be seen in Figure 1; this behaviour was also observed by other researchers (Homescu et al., 2002; He et al., 2000).

We try to save computational time and storage by saving the flow-field in the control time window only every other time step leading to only $300 + 500/2 = 550$ matrix inversions for the adjoint as compared to 800 in the original case. The result is also shown in Figure 2, and the gradients and objective function values are in reasonable agreement with each other, thus leading to a similar convergence history, except that in this case the local minima are slightly shifted (about 0.25 percent off) and the gradient norms only reduce to 10^{-3} at these minima. We also tried to skip time steps in the adjusting period and more time steps in the control window but this did not work as well or did not converge at all.

In Figure 3 the effect of different values of A and F on the drag coefficient for the harmonic rotation case using a fixed time step of

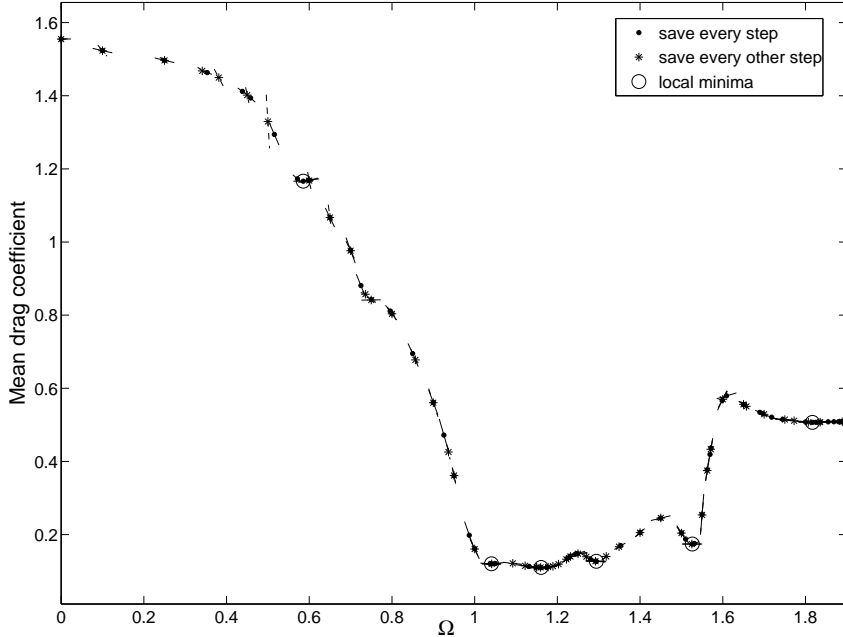


Figure 2. The design space of the constant rotating cylinder $\Omega(t) = \Omega$.

$\Delta t = 0.1$ is shown. The rotation starts smoothly, and after a transition period of about 750 steps the mean drag coefficients of the harmonically rotating cylinders are again all smaller than the mean drag coefficient of the stationary cylinder.

For this problem we use a bigger time step of $\Delta T = 0.2$ for $N^* = 375$ steps for the transition period and then switch to a smaller time step $\Delta t = 0.1$ in the actual control window for another 400 steps, yielding a total of $N = 775$ steps for each flow solve. Using the same objective function as for the constant rotating cylinder given by equation (9) and constraining the amplitude A to $[0, 1.9]$ and the frequency F to $[0, 0.3]$ to prevent rotations with excessively large amplitudes or frequencies, we can minimize the mean drag with gradient norms of about 10^{-4} at the local minima.

The resulting design space is displayed in Figure 4 with the gradients at the different design points represented by arrows, and the objective function values given by a gray scale with white representing the highest and black the lowest values. Once again several local minima can be seen, with a global minimum for $Y = Y^* \approx (0.98, 0.114)$ leading to $\bar{C}_D \approx 0.6832$, which again leads to a minimized mean drag value far beyond the extent of the control time window as can be seen in Figure 3. We did not try to skip any time steps while saving the flowfield due to the already coarse time steps for this highly oscillatory problem.

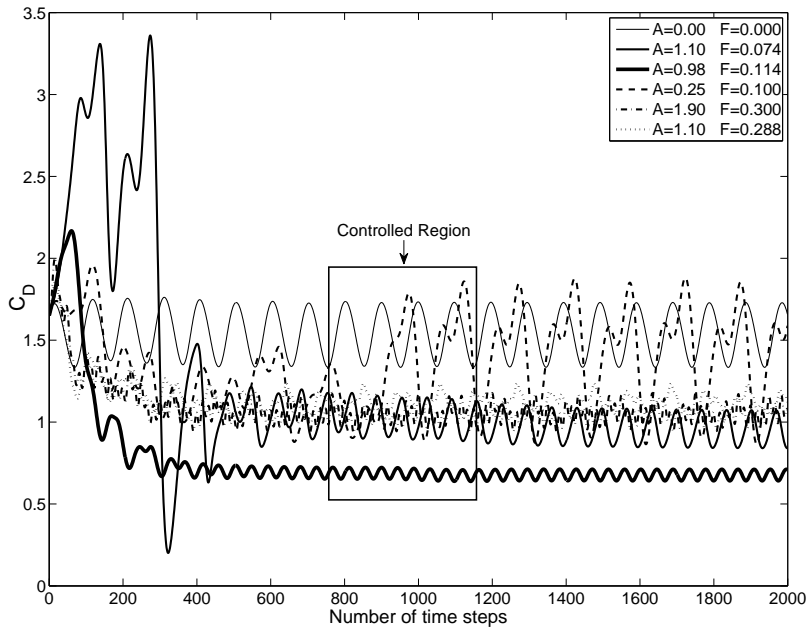


Figure 3. Drag coefficients for the harmonic rotation case for different values of A and F ($\Delta t = 0.1$).

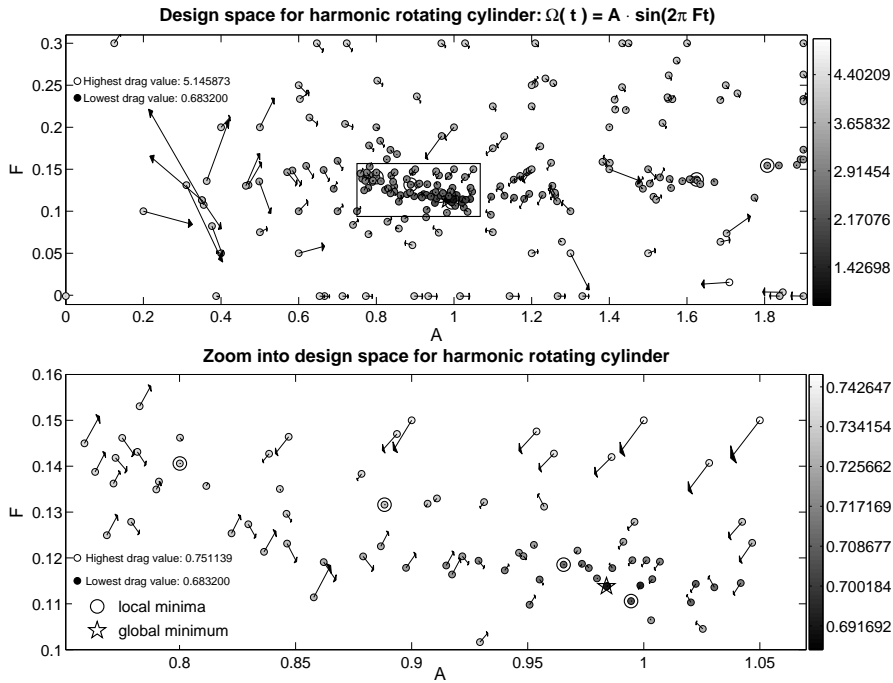


Figure 4. The design space of the harmonic rotating cylinder and a zoom into the most interesting region.

3.2. THE REMOTE INVERSE DESIGN OF A MULTI-ELEMENT AIRFOIL IN UNSTEADY LAMINAR 2D FLOW

A typical approach to tackle the high-lift noise reduction problem is to represent the CFD solution on a reasonable computational mesh that does not extend too far from the aircraft. The location of a fixed near-field plane (see Figure 5) within the computational mesh can then be specified. This near-field plane serves as an interface between the CFD solution and a wave propagation program based on principles of geometrical acoustics and nonlinear wave propagation (Lyrintzis, 2003). Such a program is able to calculate the pressure fluctuations at a user specified ground plane which can then be used as a measure of the airframe-generated noise. This paper only focuses on controlling the pressures in the near-field plane, which are one of the inputs to a wave propagation program.

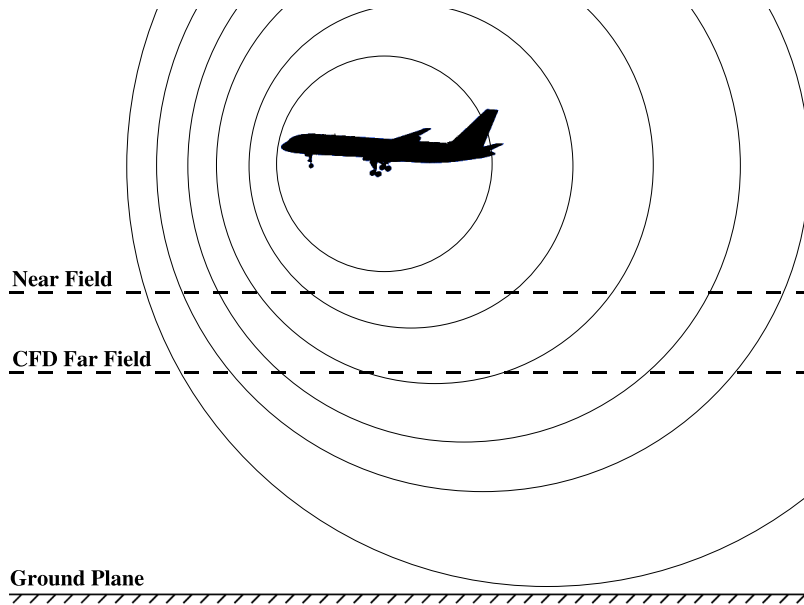


Figure 5. Schematic of the propagation of the aircraft pressure signature.

The usual adjoint implementations for shape optimization calculate a gradient for a cost function which is computed from flow variables on the surface, for example of an airfoil, that is being modified. However, for many problems, such as inlet design, turbomachinery design and airfoil-generated noise reduction, one wants to minimize an objective function using flow quantities that are not collocated at the points where the surface is being modified. This means one has to quantify the

influence of geometry modifications on the flow variables at an arbitrary location (e.g. the near-field plane) within the domain of interest. This type of remote sensitivity calculation has been successfully used before by Nadarajah *et al.* (2002; 2006; 2007) for the steady case of sonic boom minimization and by Rumpfkeil and Zingg (2007a; 2007b) for the unsteady case of turbulent flow over a single-element airfoil.

The remote inverse design test cases presented here involve the laminar flow over the multi-element NLR 7301 configuration (van den Berg, 1979). The free-stream Mach number is 0.2 with a Reynolds number of 800, and the angle of attack is 20° . At these conditions the airfoil experiences vortex shedding. We use our 2D multi-block structured solver, TORNADO (Nemec and Zingg, 2004), which is based on PROBE, to solve the underlying 2D unsteady laminar Navier-Stokes equations.

The geometries of the main element and flap are described with cubic B-spline curves (Nemec and Zingg, 2002), which means that some of the y -coordinates of the B-spline control points can easily be used as shape design variables. Furthermore, the horizontal and vertical translation of the flap can also be used as design variables. Two cases with two design variables each to keep the problem simple and to be able to compare the adjoint gradient with a finite-differenced one are considered and the shapes are displayed in Figure 6:

1. The initial airfoil is the NLR 7301, and two shape design variables of the main element are slightly perturbed to get a target airfoil.
2. The initial airfoil is the NLR 7301, and the horizontal and vertical translation design variables are slightly perturbed to get a target airfoil.

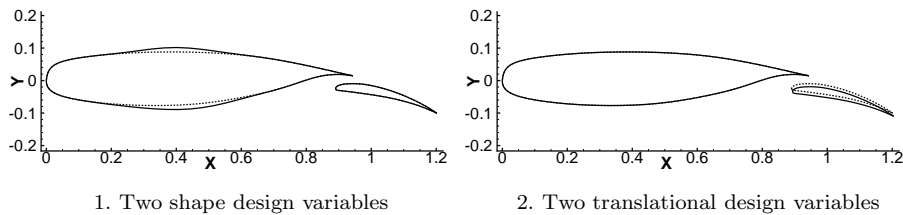


Figure 6. The initial (dashed) and target (solid) airfoils for the two test cases.

The discrete cost function J for a remote inverse design is given by

$$J = \frac{1}{2} \Delta t \sum_{n=N^*+1}^N \sum_{NF} (p^n - p^{*n})^2, \quad (10)$$

where p^n is the near-field pressure obtained from the current airfoil, and p^{*n} is the target near-field pressure obtained from the target airfoil

(both at time step n). The sum over NF implies a sum over all points that define the near-field plane, and two different choices for this plane are considered as shown in Figure 7:

- a) The near-field plane is a square that extends from -3 to 3 with a uniform spacing of 0.05 between points in both x - and y -directions.
- b) The near-field plane is a rectangle that extends from -1 to 2 in the x -direction and from -1 to 1 in the y -direction with a uniform spacing of 0.05 between points in both directions.

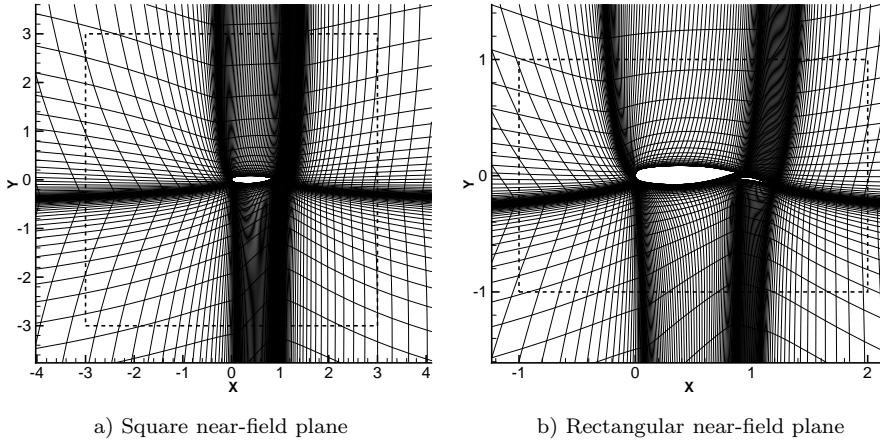


Figure 7. The grid where the two near-field planes are shown in dashed lines.

The pressures (see Figure 8) at the points of the near-field plane are calculated using biquadratic interpolation involving the closest nodes of the grid to the point in question.

Figure 9 shows the drag coefficients for the initial and target airfoils for case 1 over time using a time step of $\Delta t = 0.1$. Since the focus of this paper is to show the feasibility of an unsteady remote inverse design no grid convergence studies are performed and we are satisfied with the relative large time steps and the relative coarse grid with only about 31,000 nodes. Both flow solves are warmstarted from a NLR 7301 periodic steady state solution; thus one can see an adjustment period for the target airfoil.

Once again we want to “jump” over this unphysical adjusting period after a shape modification has taken place as quickly as possible. Therefore, we take a bigger time step $\Delta T = 0.2$ for the first $N^* = 200$ steps, and once we reach our desired control window, we use a smaller time step $\Delta t = 0.1$ for another 300 steps, for a total of $N = 500$ steps for each flow solve. The corresponding adjoint equations for this situation are again given in the Appendix.

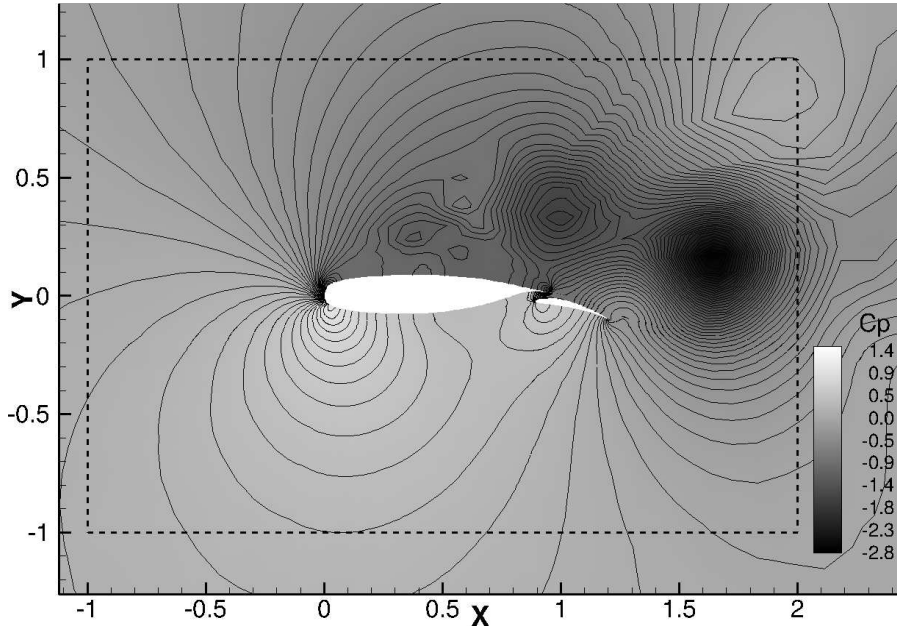


Figure 8. The pressure coefficient contours of the initial NLR 7301 configuration at $t = 0$ with the rectangular near-field plane.

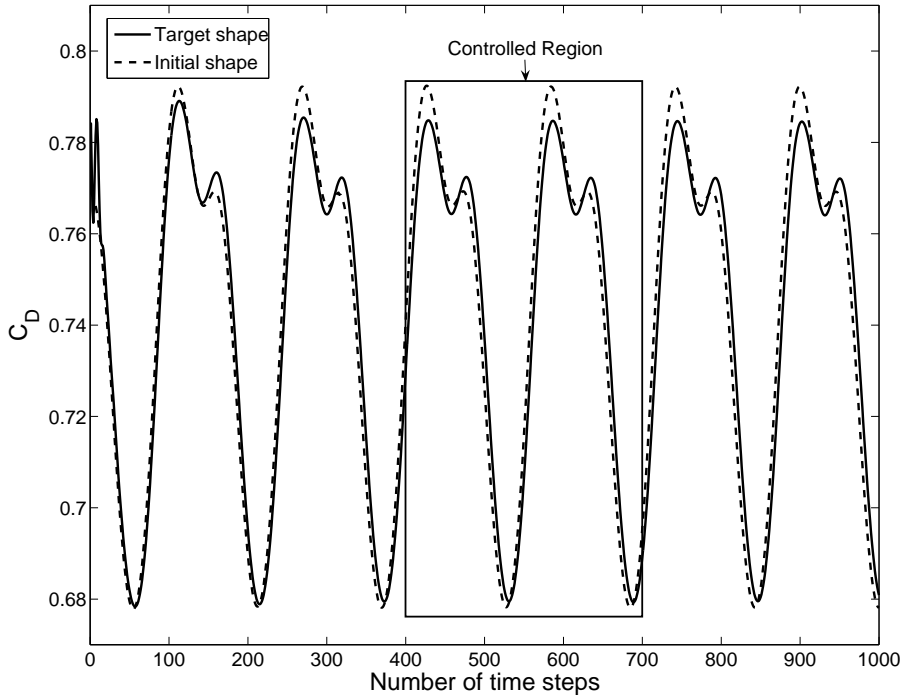


Figure 9. Drag coefficient for the initial and target airfoil for case 1 ($\Delta t = 0.1$).

The convergence histories of these remote inverse design problems with the adjoint approach in comparison to a second-order central finite-difference approach with a step size of $h = 10^{-7}$ are shown in Figure 10 for case 1 and in Figure 11 for case 2. The objective function J is always scaled such that its initial value is unity. One can see that the two approaches show a reasonable agreement, which means that our adjoint approach for the gradient calculation is accurate.

We also try to save computational time and storage by saving the flowfield in the adjusting period and in the control window only every fourth and even only every tenth time step for case 1, leading to only $500/4 = 125$ and $500/10 = 50$ matrix inversions for the solution of the adjoint equations, respectively. The result is shown in Figure 10, and the gradients and objective function values are in reasonable agreement with the original adjoint and finite-difference approach, thus leading to a somewhat similar convergence history while saving considerable computational resources.

Trying the same approach for case 2, namely saving the flowfield only every fourth and tenth time step, shows a slightly different result as displayed in Figure 11. This time the optimizer fails to converge if it uses only the information from every tenth time step. However, the information from only every fourth time step is still sufficient to converge in a similar manner as the original adjoint. We also save the flowfield only every fifth time step and one can see that this approach still works, although it comes with a huge increase in optimization iterations for the case 2a.

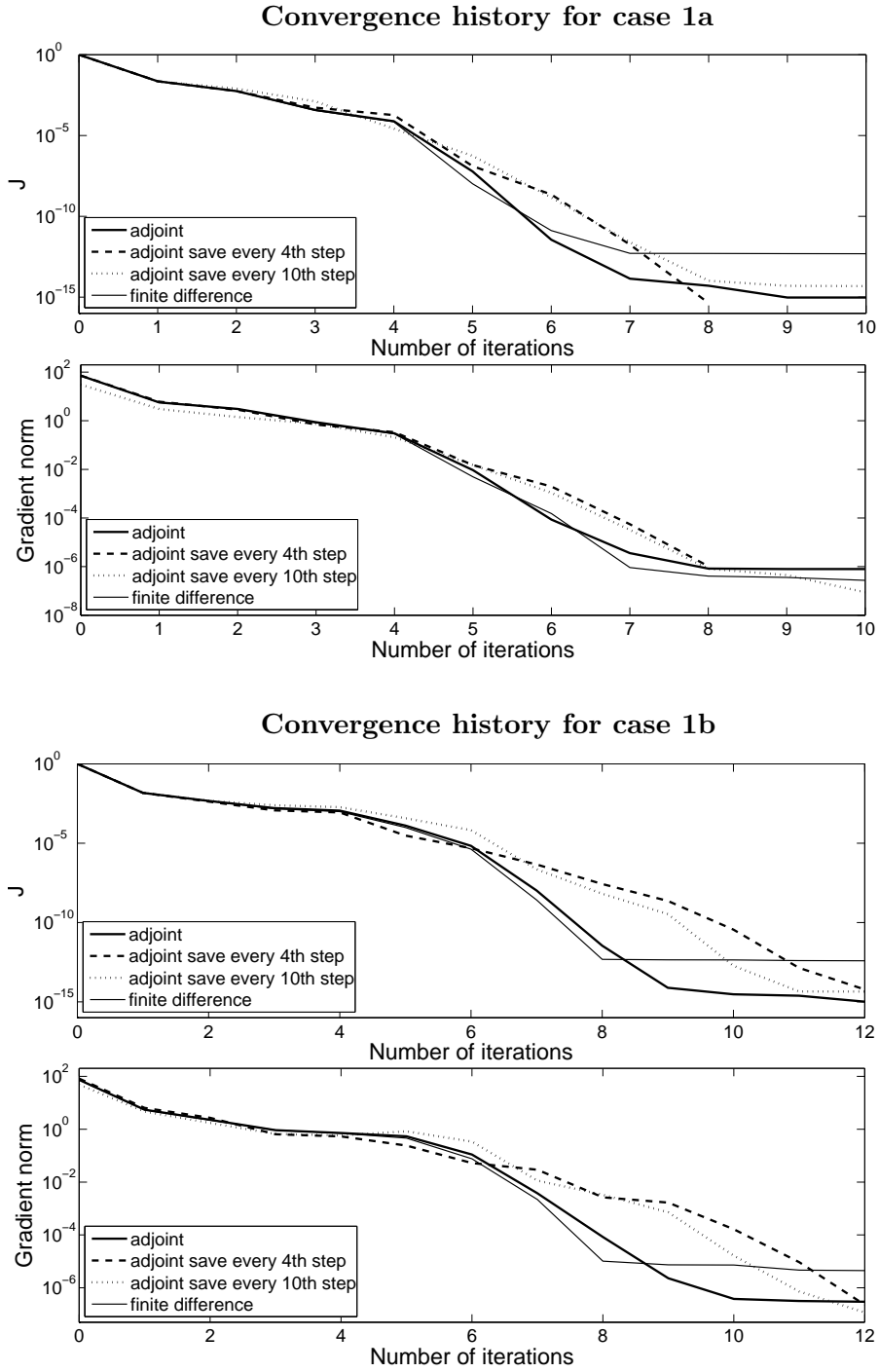


Figure 10. Convergence histories of the remote inverse design problem with two shape design variables.

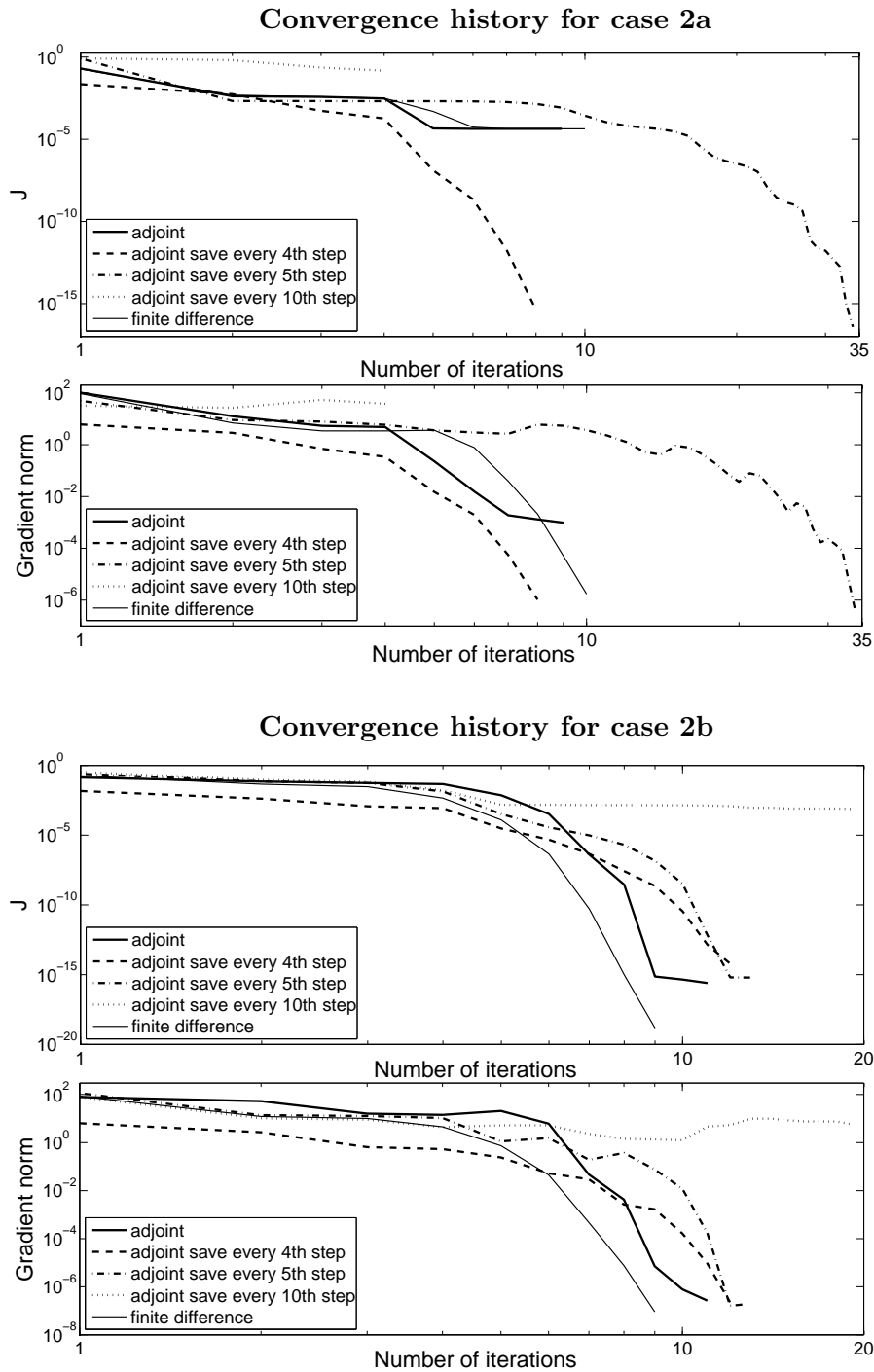


Figure 11. Convergence histories of the remote inverse design problem with two translational design variables (Note the log scale on both axes).

4. Conclusion

A general framework to derive a discrete adjoint method for the optimal control of unsteady flows was presented. It was shown that marching with a bigger time step over transitional or unphysical adjusting periods as well as skipping time steps (e.g. every other) while recording the flow solution works well in practice, thus resulting in significant savings in both memory and computational time for unsteady optimization problems. Our future work will focus on the ability to modify the shape of an airfoil to minimize the radiated noise while maintaining good performance. Therefore, we will investigate the presented remote inverse design problem further by using more design variables, a more realistic turbulent flow and by implementing a near to far-field wave propagation method.

Acknowledgements

The funding of the second author by the Natural Sciences and Engineering Research Council of Canada and the Canada Research Chairs program is gratefully acknowledged.

Appendix

In this appendix, the discrete adjoint equations are derived in the form in which they are used to present all the results in this paper. The time-marching method of choice is the second-order accurate implicit backward difference (BDF2) method, the flow is controlled after a certain transition period and one can use different time step sizes in the transition period and the control window.

The unsteady flow solve is warmstarted at some point in time which means that Q^0 and Q^{-1} are known. In order to “jump” over the adjusting or transition period as quickly as possible, a bigger time step ΔT for N^* steps is used. Once the domain where the problem is supposed to be controlled is reached, a smaller time step Δt for another $N - N^*$ steps is used for a total of N steps. To maintain the second-order time accuracy through this time step size change, the time-dependent flow solution Q^n is implicitly defined via the following unsteady residuals:

$$R^{*n}(Q^n, Q^{n-1}, Q^{n-2}, Y) := \frac{3Q^n - 4Q^{n-1} + Q^{n-2}}{2\Delta T} + R(Q^n, Y) = 0$$

for $n = 1, \dots, N^*$

$$\begin{aligned}
R^{*N^*+1}(Q^{N^*+1}, Q^{N^*}, Q^{N^*-1}, Y) &:= \frac{2\Delta t + \Delta T}{\Delta t(\Delta t + \Delta T)} Q^{N^*+1} - \frac{\Delta t + \Delta T}{\Delta t \Delta T} Q^{N^*} \\
&\quad + \frac{\Delta t}{\Delta T(\Delta t + \Delta T)} Q^{N^*-1} + R(Q^{N^*+1}, Y) = 0 \\
R^{*n}(Q^n, Q^{n-1}, Q^{n-2}, Y) &:= \frac{3Q^n - 4Q^{n-1} + Q^{n-2}}{2\Delta t} + R(Q^n, Y) = 0 \\
&\quad \text{for } n = N^* + 2, \dots, N.
\end{aligned}$$

The problem of minimizing a discrete objective function given by $J = \sum_{n=N^*+1}^N I^n(Q^n, Y)$ is then equivalent to the unconstrained optimization problem of minimizing the Lagrangian function

$$\mathcal{L} = \sum_{n=N^*+1}^N I^n(Q^n, Y) + \sum_{n=1}^N (\psi^n)^T R^{*n}(Q^n, Q^{n-1}, Q^{n-2}, Y)$$

with respect to Q^0, \dots, Q^N and ψ^1, \dots, ψ^N . This leads to the following equations for ψ^n :

$$\begin{aligned}
0 &= (\psi^n)^T \nabla_{Q^n} R^{*n} + (\psi^{n+1})^T \nabla_{Q^n} R^{*n+1} + (\psi^{n+2})^T \nabla_{Q^n} R^{*n+2} \\
&\quad \text{for } n = 1, \dots, N^* \\
0 &= \nabla_{Q^n} I^n + (\psi^n)^T \nabla_{Q^n} R^{*n} + (\psi^{n+1})^T \nabla_{Q^n} R^{*n+1} + (\psi^{n+2})^T \nabla_{Q^n} R^{*n+2} \\
&\quad \text{for } n = N^* + 1, \dots, N-2 \\
0 &= \nabla_{Q^{N-1}} I^{N-1} + (\psi^N)^T \nabla_{Q^{N-1}} R^{*N} + (\psi^{N-1})^T \nabla_{Q^{N-1}} R^{*N-1} \\
0 &= \nabla_{Q^N} I^N + (\psi^N)^T \nabla_{Q^N} R^{*N},
\end{aligned}$$

which can be written equivalently as

$$\begin{aligned}
\psi^N &= -((\nabla_{Q^N} R^{*N})^T)^{-1} [(\nabla_{Q^N} I^N)^T] \\
\psi^{N-1} &= -((\nabla_{Q^{N-1}} R^{*N-1})^T)^{-1} [(\nabla_{Q^{N-1}} I^{N-1})^T + (\nabla_{Q^{N-1}} R^{*N})^T \psi^N] \\
\psi^n &= -((\nabla_{Q^n} R^{*n})^T)^{-1} \left[(\nabla_{Q^n} I^n)^T + (\nabla_{Q^n} R^{*n+1})^T \psi^{n+1} \right. \\
&\quad \left. + (\nabla_{Q^n} R^{*n+2})^T \psi^{n+2} \right] \quad \text{for } n = N-2, \dots, N^* + 1 \\
\psi^n &= -((\nabla_{Q^n} R^{*n})^T)^{-1} \left[(\nabla_{Q^n} R^{*n+1})^T \psi^{n+1} + (\nabla_{Q^n} R^{*n+2})^T \psi^{n+2} \right] \\
&\quad \text{for } n = N^*, \dots, 1.
\end{aligned}$$

A little care must be taken in calculating derivatives of R^{*N^*+1} with respect to Q^n since the factors in front of Q^{N^*+1} , Q^{N^*} and Q^{N^*-1} slightly differ from the usual scheme. Finally, the gradient of J with respect to the design variables Y is given by

$$\frac{\partial J}{\partial Y} = \frac{\partial \mathcal{L}}{\partial Y} = \sum_{n=N^*+1}^N \nabla_Y I^n(Q^n, Y) + \sum_{n=1}^N (\psi^n)^T \nabla_Y R(Q^n, Y).$$

References

- Anderson, W. K. and D. L. Bonhaus: 1999, 'Airfoil Design on Unstructured Grids for Turbulent Flows'. *AIAA Journal* **Vol. 37, No. 2**, pp. 185–191.
- Broyden, C.: 1970, 'The Convergence of a Class of Double-Rank Minimization Algorithms'. *Journal Inst. Math. Applic.* **Vol. 6**, pp. 76–90.
- Byrd, R. H., P. Lu, J. Nocedal, and C. Zhu: 1995, 'A Limited Memory Algorithm for Bound Constrained Optimization'. *SIAM J. Scientific Computing* **16 Vol. 5**, pp. 1190–1208.
- Cox, J., K. Brentner, and C. Rumsey: 1998, 'Computation of Vortex Shedding and Radiated Sound for a Circular Cylinder: Subcritical to Transcritical Reynolds Numbers'. *Theoretical and Computational Fluid Dynamics* **Vol. 12**, pp. 233–253.
- Duta, M., M. Giles, and M. Campobasso: 2002, 'The Harmonic Adjoint Approach to Unsteady Turbo Machinery Design'. *International Journal for Numerical Methods in Fluids* **Vol. 40**, pp. 323–332.
- Fletcher, R.: 1970, 'A New Approach to Variable Metric Algorithms'. *Computer Journal* **13**, pp. 317–322.
- Goldfarb, D.: 1970, 'A Family of Variable Metric Updates Derived by Variational Means'. *Mathematics of Computing* **Vol. 24**, pp. 23–26.
- He, J.-W., R. Glowinski, R. Metcalfe, A. Nordlander, and J. Periaux: 2000, 'Active Control and Drag Optimization for Flow past a Circular Cylinder'. *Journal of Computational Physics* **Vol. 163**, pp. 83–117.
- Henderson, R.: 1997, 'Nonlinear Dynamics and Patterns in Turbulent Wake Transition'. *Journal of Fluid Mechanics* **Vol. 352**, 65.
- Homescu, C., I. Navon, and Z. Li: 2002, 'Suppression of Vortex Shedding for Flow around a Circular Cylinder Using Optimal Control'. *Int. Journal for Num. Meth. Fluids* **Vol. 38**, pp. 43–69.
- Isono, S. and D. Zingg: 2004, 'A Runge-Kutta-Newton-Krylov Algorithm for Fourth-Order Implicit Time Marching Applied to Unsteady Flows'. AIAA, 2004-0433.
- Jameson, A.: 1995, 'Optimum Aerodynamic Design Using Control Theory'. In: *Computational Fluid Dynamics Review*, Hafez, M., Oshima, K. (eds). Wiley: New York, pp. 495–528.
- Jameson, A., N. Pierce, and L. Martinelli: 1998, 'Optimum Aerodynamic Design Using the Navier-Stokes Equations'. *Theoretical and Computational Fluid Dynamics* **Vol. 10, No. 1**, pp. 213–237.
- Khorrami, M., M. Berkman, and M. Choudhari: 2000, 'Unsteady Flow Computations of a Slat with a Blunt Trailing Edge'. *AIAA Journal* **Vol. 38, No. 11**, pp. 2050–2058.
- Lyrantzis, A. S.: 2003, 'Surface Integral Methods in Computational Aeroacoustics - From the (CFD) Near-Field to the (Acoustic) Far-Field'. *Aeroacoustics* **Vol. 2(2)**, pp. 95–128.
- Mani, K. and D. J. Mavriplis: 2007, 'An Unsteady Discrete Adjoint Formulation for Two-Dimensional Flow Problems with Deforming Meshes'. AIAA, 2007-60.
- Nadarajah, S. and A. Jameson: 2002, 'Optimal Control of Unsteady Flows using a Time Accurate Method'. AIAA, 2002-5436.
- Nadarajah, S., A. Jameson, and J. Alonso: 2002, 'An Adjoint Method for the Calculation of Remote Sensitivities in Supersonic Flow'. AIAA, 2002-0261.
- Nadarajah, S., A. Jameson, and J. Alonso: 2006, 'An Adjoint Method for the Calculation of Remote Sensitivities in Supersonic Flow'. *International Journal of Computational Fluid Dynamics* **Vol. 20(2)**, pp. 61–74.

- Nadarajah, S., O. Soucy, and C. Balloch: 2007, ‘Sonic Boom Reduction via Remote Inverse Adjoint Approach’. AIAA, 2007-56.
- Nemec, M. and D. Zingg: 2002, ‘Newton-Krylov Algorithm for Aerodynamic Design Using the Navier-Stokes Equations’. *AIAA Journal* **Vol. 40, No. 6**, pp. 1146–1154.
- Nemec, M. and D. Zingg: 2004, ‘Multipoint and Multi-Objective Aerodynamic Shape Optimization’. *AIAA Journal* **Vol. 42, No. 6**, pp. 1057–1065.
- Obayashi, S.: 1997, ‘Aerodynamic Optimization with Evolutionary Algorithms’. Inverse Design and Optimization Methods, Lecture Series 1997-05, edited by R. A. V. den Braembussche and M. Manna, Von Karman Institute for Fluid Dynamics, Brussels.
- Pueyo, A. and D. Zingg: 1998, ‘Efficient Newton-Krylov Solver for Aerodynamic Computations’. *AIAA Journal* **Vol. 36, No. 11**, pp. 1991–1997.
- Pulliam, T. H.: 1986, ‘Efficient Solution Methods for the Navier-Stokes Equations’. Lecture Notes for the Von Karman Institute For Fluid Dynamics Lecture Series.
- Rumpfkeil, M. and D. Zingg: 2007a, ‘A General Framework for the Optimal Control of Unsteady Flows with Applications’. AIAA, 2007-1128.
- Rumpfkeil, M. and D. Zingg: 2007b, ‘The Remote Inverse Shape Design of Airfoils in Unsteady Flows’. Proceedings of the 12th Annual CASI Aerodynamics Symposium, Toronto, paper 318.
- Saad, Y. and M. Schultz: 1986, ‘GMRES: A Generalized Minimal Residual Algorithm for Solving Nonsymmetric Linear Systems’. *SIAM Journal on Scientific and Statistical Computing* **Vol. 7 No. 3**, 856–869.
- Shanno, D.: 1970, ‘Conditioning of Quasi-Newton Methods for Function Minimization’. *Mathematics of Computing* **Vol. 24**, pp. 647–656.
- Singer, B., K. Brentner, and D. Lockard: 2000, ‘Computational Aeroacoustic Analysis of Slat Trailing-Edge Flow’. *AIAA Journal* **Vol. 38, No. 9**, pp. 1558–1564.
- Singer, B. and Y. Guo: 2004, ‘Development of Computational Aeroacoustics Tools for Airframe Noise Calculations’. *International Journal of Computational Fluid Dynamics* **Vol. 18(6)**, pp. 455–469.
- Tatossian, C. and S. Nadarajah: 2007, ‘Optimum Shape Design of Helicopter Rotors in Forward Flight via Control Theory’. AIAA, 2007-3951.
- Tokumaru, P. and P. Dimotakis: 1991, ‘Rotary Oscillation Control of a Cylinder Wake’. *Journal of Fluid Mechanics* **Vol. 224**, 77.
- van den Berg, B.: Jan. 1979, ‘Boundary Layer Measurements on a Two-Dimensional Wing with Flap’. National Aerospace Lab, NLR TR 79009 U, Amsterdam.
- van der Vorst, H.: 1992, ‘Bi-CGSTAB: A Fast and Smoothly Converging Variant of Bi-CG for the Solution of Nonsymmetric Linear Systems’. *SIAM Journal on Scientific and Statistical Computing* **Vol. 13**, 631–644.
- von Karman, T.: 1911, ‘Ueber den Mechanismus des Widerstandes den ein bewegter Koerper in einer Fluessigkeit erzeugt’. *Nachr. Ges. Wiss. Goettingen Math. Phys. Klasse*, 509–517.
- Williamson, C.: 1989, ‘Oblique and Parallel Modes of Vortex Shedding in the Wake of a Circular Cylinder at Low Reynolds Numbers’. *Journal of Fluid Mechanics* **Vol. 206**, 579.
- Zhu, C., R. Byrd, P. Lu, and J. Nocedal: 1994, ‘L-BFGS-B: A Limited Memory FORTRAN Code for Solving Bound Constrained Optimization Problems’. Technical Report NAM-11, EECS Department, Northwestern University.